CEBAF Program Advisory Committee Nine Proposal Cover Sheet

This proposal must be received by close of business on Thursday, December 1, 1994 at:

CEBAF
User Liaison Office, Mail Stop 12 B
12000 Jefferson Avenue
Newport News, VA 23606

Proposal Title

High Resolution 1p shell Hypernuclear Spectroscopy

Contact Person

Name: F. Garibaldi
Institution: Physics Laboratory, I.S.S. and INFN Sezione Sanita'
Address: Viale Regina Elena 299
City, State ZIP/Country: Rome, Italy 00161
Phone: +396 49902243 **FAX:** +396 446 2872
E-Mail — Internet: GARIBALDI@VAXSAN.ISS.INFN.IT

Experimental Hall: A **Days Requested for Approval:** _____

Hall B proposals only, list any experiments and days for concurrent running:

CEBAF Use Only

Receipt Date: 12/15/94 PR 94-107

By: _____

High Resolution Hypernuclear 1p shell Spectroscopy

S. Frullani, F. Garibaldi
ISS and INFN/Sanita', Rome, Italy

P. Markowitz
University of Maryland, College Park, Maryland

T. Saito
Tohoku University, Japan

Hall A Collaboration Proposal

MIT, Cambridge Massachusetts *INFN/Bari, Bari, Italy*
INFN/Lecce, Lecce, Italy
The University of Virginia, Charlottesville, Virginia
Yerevan Physics Institute, Yerevan, Armenia
University of Georgia, Athens Georgia
American University, Washington
Rutgers University, New Jersey
The College of William and Mary, Williamsburg, Virginia
California State University, California
University of New Hampshire, New Hamphire
Norfolk State University, Norfolk, Virginia
Hampton University, Hampton, Virginia
Nuclear Physics Institute , 25068 Rez/Prague, Czech Republic

December 15, 1994

Current:	Targets:	Beam Energies:	Beam Time:
100 μA	Solid, Waterfall	4 GeV	580 hours

Appendix: Participants

E. Cisbani	J. Lerose
J. Calarco	R. Lourie
O.K. Baker	K. Maeda
W. Bertozzi	R. Michael
P. Markowitz	G.C. Chang
S. Nanda	J.P.Chen
E.A.J.M Offerman	R. Perrino
R. De Leo	V.Punjabi
R.D. Ransome	P.M. Rutt
M. Finn	E. Nappi
B. Flanders	A. Saha
S. Frullani	T Saito
F. Garibaldi	T. Scognetti
A. Gasparian	A. Sarty
S. Gilad	M. Sotona
M. Iodice	G.M. Urciuoli
H Voskanian	B. Wojosetkhowski
A. Leone	L. Tang

ABSTRACT

The goal to study hypernuclear systems with high resolution has been pursued in several Laboratories for many years due to the information on the spin dependence of the effective Λ-N interaction that can be obtained from the energy splitting of hypernuclear spin doublets. At the moment only the electromagnetic production of hypernuclei with electron beam of CEBAF quality together with the high resolution spectrometers of the Hall A to detect scattered electrons and the produced kaons can afford the possibility to obtain high resolution data (280 keV) on hypernuclear spectra as well as precise informations on the nuclear-hypernuclear transition.

To obtain maximum cross section, the electron scattering angle has to be as small as possible (large virtual photon flux) and kaon angle close to the virtual photon direction where the moemntum transfer is minimum. This means that it is s a crucial requirement to have $\Theta_e <$ 10°, and $| \Theta_k - \Theta_\gamma | < 10$ °.

This proposal is based on the PR-93015 proposal presented, among other, for a program to be carried out using the Multi Particle Spectrometer (MPS) proposed at that time.

Our present calculations show that hypernuclear spectroscopy can be done with small modifications to the existing devices in hall A, at the cost of less good resolution (≈ 280 keV instead of ≈ 100 keV), but still *about an order of magnitude better than what can be obtained with presnt devices, also at CEBAF*. This allows obtaining very important physics informations.

The PAC put two questions about feasibility of the PR-93015 experiment: 1) the cross sections for electroproduction are unknown and, 2) the single rates are very high.

The hypernuclear electroproduction cross sections contain two main ingredients : a) the lementary electroproduction of Λ off proton; b) the nuclear transition from the target nucleus to the final hypernuceus.

For the "nuclear" part of cross-section, the reliability of the DWIA type calculations was checked in other hypernuclear production reactions (K^-, π^-) and, especially, (π^+, K^+) where the kinematics is similar to our kinematics. The measured cross sections are explained satisfactorily.

For the elementary process part a new set of coupling constant has been used, taken form a model fitting simultaneously to all available photo - and electroproduction data up to the (virtual) photon energy $E\gamma \approx 2.2$ GeV (used in the present proposal). The model dependence of our calculation is rather small.

The single rates have been reevaluated by a new code better tested and checked for the new kinematics . They are reasonable, ~ two order of magnitude smaller than in the previous proposal, so they are not a problem for the standard HRS detector package .

It can be shown that, in hall A, by moving the scattering chamber upstream and putting

two septa for the electron and hadron arm, it is possible to get $\Theta_e = \Theta_k = 6°$, at a reasonable cost. These devices are thought to be provided by Institutions external to USA.

We have to emphasize that there is an obvious advantage for many experiments in Hall A to going to the most forward angle, namely for the class of experiments measuring parity violating asymmetries.

Physics motivations and a first experimental program on this subject are presented as part of a physics program that can be done in Hall A.

1. Introduction

Hypernuclear physics is currently an important and exciting part of intermediate energy physics. The Λ-hypernucleus, a nuclear system with the strangeness S = -1, in which the Λ-hyperon replaces one of the nucleons is a long-living baryon system ($\tau \sim 10^{-10}$ s) and provides us with a variety of nuclear phenomena. The hyperon is not excluded from the filled nucleon orbitals by Pauli principle and can penetrate deep inside the nucleus. Weak interactions in the nuclear medium (mesonic $\Lambda \Rightarrow N + \pi$ versus nonmesonic $\Lambda + N \Rightarrow N + N$ decay modes of hypernucleus) can be studied as well as possible modifications of baryon properties (e.g., the magnetic moment of Λ) in the nuclear environment. From low-energy Λp scattering studies [1] we obtained information about the s-state ΛN interaction but the non-central part of ΛN forces is not well established. The better systematics of hypernuclear spectroscopy can help to learn more about the ΛN interaction. Especially useful information on the spin dependence of the effective ΛN interaction can be obtained from the energy splitting of hypernuclear spin doublets.

The theory of low-lying 1p-shell hypernuclear states was restricted for a long time to use the photoemulsion and bubble chamber data on the hypernuclear ground states [2].

Most of the currently available information on hypernuclear excited states comes from the strangeness exchange reaction $K^- + n \Rightarrow \pi^- + \Lambda$ with the kaon beam momenta p_K = 400 - 450 MeV/c or p_K = 700 - 800 MeV/c. The momentum transferred to the target nucleus is small (q < 100 MeV/c) and the spin-flip transitions for forward pion angles $\Theta_\pi < 10^o$ are negligible in this energy region so that the $\Delta l = \Delta s = 0$ transitions dominate. Due to the strong absorption of the kaon and pion, the reaction takes place on peripheral nucleons. As a result, the substitutional states are predominantly populated. As a rule, the substitutional states lie in the continuum and their interpretation in the framework of the standard shell model calculations is not straightforward.

In the associated production reaction $\pi^+ + n \Rightarrow K^+ + \Lambda$ the momentum transferred is as high as q = 350 MeV/c at p_π = 1.05 GeV/c (the maximum in the elementary cross section). The spin flip part of the elementary amplitude is strong enough to produce an appreciable polarization in the final hypernuclear states [3] but still weak at $\Theta_K < 10^o$, so that the $\Delta l = 1, 2$ and $\Delta s = 0$ transitions are favoured. It means, that also $p_N \Rightarrow s_\Lambda$ transitions are prefered, but, due to the lack of the sufficiently strong spin flip, only lower members of the hypernuclear bound states are populated [3]

In the stopped kaons (K^-_{stop}, π) reaction the energy of incoming kaon is well defined (E_k=0), the energy resolution is determined by the pion detecting system. The momentum trasferred to the nucleus is ≈ 250 MeV/c (comparable with (π+, K+) case, so that $\Delta l = 1, 2$ transition dominate. Spin flip is very weak. In ^{12}C, J = 1- g.s. and a group of (undistinguishable) J=2+ states at Ex ~ 10.5 MeV are visible.

The energy resolution of all these processes is typically of the order of 2 MeV or more, the value which is much greater than characteristic spin doublet splitting.

Only the electromagnetic (electro - and photo -) production of strangeness on the electron beam of CEBAF quality afford the possibility to obtain the high resolution data on hypernuclear spectra :

(1) the quality of CEBAF beam (high intensity and energy resolution) make possible to identify the bound hypernuclear levels with a resolution ≈ 280 keV.

(2) due to the strong spin flip contribution, both the members of spin doublet may be populated,

(3) in contrast with (K^-, π^-) and (π^+, K^+), electromagnetic production of $K^+\Lambda$ pair goes on the proton making possible to study the hypernuclei non available otherwise ($^7He_\Lambda$, $^9Li_\Lambda$,....),

(4) a possible production of the controversial Σ - hypernuclei may be another interesting problem for the electroproduction of strangeness since the Λ and Σ production rates are comparable.

A typical example (^{12}C target) of the spectroscopic information which can be obtained from (K^-,π^-), (π^+,K^+) and $(e,e'K^+)$ reactions is shown in Fig. 1.

2. Shell model description of hypernuclear spectra

The many particle shell model is used, by analogy with spectroscopy of light nuclei, to describe the 1p-shell hypernuclear spectra quantitatively in terms of the $|s^4p^{A-5} * s_\Lambda ; JT\rangle$ configurations. As was shown many times [4-5], the available hypernuclear data from (K^-, π^-), $(K^-, \pi^-\gamma)$ and (π^+, K^+) may be adequately described by weak coupling model. In this model the Λ-hyperon in 0s shell is coupled to a certain nuclear state of the parent nucleus with spin and parity J_{A-1} , π creating a doublet of states $J = J_{A-1} \pm 1/2$. Hypernuclear states belonging to different doublets mix only weakly, as a rule, and doublet energy splitting is therefore determined by spin dependent part of the effective ΛN interaction alone.

Previous attempts to investigate the spin dependence of the ΛN effective interaction in light hypernuclei were limited by a lack of data. In the first serious phenomenological analysis [4] 12 ground state energies together with the constraints imposed by a knowledge of three ground states spins were used as a data input to the fit. The optimum version (called *canonical* in [5]) predicts rather large doublet splittings (≈ 1 MeV - see Fig's 2-5, model C).

The later experiments [6-7] where γ-lines from $^7Li_\Lambda$ and $^9Be_\Lambda$ in $(K^-, \pi^-\gamma)$ reaction were measured, have not confirmed the position of $5/2^+$ level in $^7Li_\Lambda$ (predicted by canonical set at 1.35 MeV; $E_{exper} = 2.034 \pm 0.023$ MeV) and the strong splitting of $(3/2^+,5/2^+)$ first excited doublet in $^9Be_\Lambda$ ($\delta = 3.66(5/2^+) - 2.09(3/2^+) = 1.57$ MeV; in the experiment only one γ-line

was detected with E = 3.08 MeV).

To overcome the difficulties, Millener, Gal, Dover and Dalitz [8] proposed an alternative set of parameters (*standard* - S). The predicted doublet splittings, compared with the canonical set (C), are much smaller (see Fig's. 2-5, model S). Guided by the predictions of the doublet splittings in the 1p-shell hypernuclei, the BNL experimental group made an attempt to detect the γ-transitions $2^- \Longrightarrow 1^-$(gr. st.) with $E_\gamma = 170$ keV in $^{10}B_\Lambda$ and $1^- \Longrightarrow 0^-$ (gr.st.) with $E_\gamma = 80$ keV in $^{16}O_\Lambda$ [9-10]. No such hypernuclear γs were observed between 80 to 510 keV

As a solution of the puzzle, another set of parameters was proposed by Majling, Fetisov, Zofka and Eramzhyan (*FMZE*) [11] (see Fig's. 2-5, model FMZE).

The *weak coupling model* [8,11] of hypernuclear structure is now commonly accepted. In this model:

(1) spin-doublet splittings are rather small, generally of the order some hundred keV or smaller.

(2) energy splittings between different spin doublets follow very closely the energy spectrum of the underlying "parent" nucleus.

Still, recent KEK experiment [12] on $^{12}C_\Lambda$ production in (π^+, K^+) reaction questions this picture seriously. In the experiment two peaks were clearly observed in addition to the well known ones, which correspond to the ground state of $^{12}C_\Lambda$ and to the group of (p^{-1}, p^Λ) $J = 2^+$ states at excitation energy $E_X \approx 10.8$ MeV. These additional peaks are interpreted as $J = 1^-$ hypernuclear states based on ^{11}C low-lying excited states $J = 1/2^-$, and $J = 3/2^-$ having energies E = 2 MeV and E = 4.80 MeV respectively. However, the energy positions of both peaks: $E = 2.61 \pm 0.134$ Me`V and $E = 6.81 \pm 0.28$ MeV are in sharp disagreement with predictions of weak coupling model - see Fig. 6.

Weak spin-dependence of ΛN residual interaction may be only hardly understood also from recent OBEP models of hyperon-nucleon interaction. The calculations of hypernuclear spectra based on reaction matrix approach show, on the contrary, very strong spin dependence [13].

Situation in hypernuclear spectroscopy is therefore far from being satisfactory. The elctromagnetic production of strange mesons is very promising tool in this respect.

3. Electroproduction of hypernuclei

Our estimates of the electroproduction cross-sections on ^{7}Li, ^{9}Be, ^{12}C and ^{16}O targets are based on the following assumptions (see also [14]):

1) (e,e'K^+) production rates are calculated in distorted waves impulse approximation (DWIA). Kaon distortion is calculated in eikonal approximation ($p_K \approx 1$ GeV/c, relatively weak

absorption by nuclei) with lowest order optical potential determined by the target nucleus density and by the appropriately averaged kaon-proton and kaon-neutron forward scattering amplitude. For KN scattering, Martin parametrization [15] is used. The quality of the DWIA type calculations was checked in other hypernuclear production reactions (K^-, π^-) and, especially, (π^+, K^+) with a comparable momentum transfer to the target nucleus ($q \approx 350$ MeV/c). The measured cross-sections are explained satisfactorily as it is illustrated in Fig. 7 from Ref. [16] for (π^+, K^+) production of $^{12}C_\Lambda$ hypernucleus.

2) for the elementary process $e + P \Longrightarrow e' + \Lambda + K$ the electroproduction models based on effective Lagrangian theory with strong coupling constants fitted to available photoproduction data. The models are fitted, as a rule, to the medium energy (E_γ from the threshold $E_{thr} = 911$ MeV to $E_\gamma = 1.4$ GeV) photoproduction data only. Recently, Williams et al. [17] published the new set of coupling constants for a model fitted simultaneously to all available photo- and electroproduction data up to the (virtual) photon energy $E\gamma \approx 2.2$ GeV. The quality of the fit is illustrated in Fig's. 8,9 reproduced from [17]. This crossing and duality constrained model is then used as a standard choice in our estimations.

3) shell model nuclear and hypernuclear wave functions are calculated with effective NN interaction of Utrecht group [18] including the $1\hbar\omega$ opposite parity states. As an effective ΛN interaction we use the one derived [13] from Nijmegen soft core hyperon - nucleon interaction. It means that our ΛN effective interaction contain no free parameteres, but Fermi momentum (nuclear density).

Momentum transfer to the hypernucleus in the electroproduction is rather large ($q \sim 350$ MeV/c for light nuclei) and decreases steadily with increasing energy of virtual photon $E_\gamma = E_e - E_{e'}$. The elementary photoproduction cross section, with K at forward angles, is almost constant for $E_\gamma = 1.2$ - 2.2 GeV (see DESY data, Fig. 8). The momentum transfer for forward kaon scattering angles fall down from $q \approx 330$ MeV/c at $E_{\gamma virt} = 1.2$ GeV to $q \approx 250$ MeV/c at $E_{\gamma virt} = 2.5$ GeV (^{16}O target) and it means that higher energies would be preferable. The dependence of the production cross section for $J = 2^-$, $E = 7.03$ MeV state of $^{16}N_\Lambda$ on virtual photon energy is shown in Fig. 10. Energy of scattered electrons $E_{e'} = 1.3$ GeV is kept constant, electron scattering angle $\Theta_e = 7^o$ and kaon scattering angle $\Theta_K = \Theta_\gamma$ (in the virtual photon direction). Triple differential cross-section increases steadily with increasing virtual photon energy as it realy should be. The cross section is presented for two different models of elementary electroproduction process: the standard one discussed above (LC4) and the elder one (C3) [19] which describe the available data (Fig's. 8,9) also well. The difference between two models illustates the possible model dependence of our estimates.

At last, Fig's. 11-14 show the calculated strength functions at $E_e = 4$ GeV, $E_{e'} = 1.8$ GeV, $\Theta_e = 6^\circ$ and $\Theta_K = 6^\circ$, for ^7Li, ^9Be, ^{12}C and ^{16}O targets. On these kinematical conditions virtual photons are almost "real" ($q^2 = -0.00789 GeV^2$), with polarization $\varepsilon = 0.745$

and virtual photon flux $\Gamma = 0.0183$ GeV^{-2}. In all cases the LC4 [17] electroproduction model is used and energy resolution of 0.3 MeV is supposed for bound hypernuclear levels. For unbound levels (above the strong decay threshold) the uniform escape width $\Gamma = 2$ MeV is assumed.

In $^{7}He_{\Lambda}$ (Fig. 13), *which has never been created,* the $J = 1/2^{+}$ ground state is strongly populated. The predicted production rates for $3/2^{+}$ and $5/2^{+}$ members of the first excited doublet (built on $J=2^{+}$, E=1.8 MeV first excited state of ^{6}He core nucleus) are comparable but smaller. In addition, the doublet splitting predicted by weak coupling models is much smaller (≈10 keV) than in our case (YNG interaction) and could not be distinguished with energy resolution of few hundred keV. All higher hypernuclear states are unbound (neutron decay threshold $E_{thr} = 2.9$ MeV). Nevertheless, the doublet of $^{7}He_{\Lambda}$ states $J=3/2^{+}$, $5/2^{+}$ at excitation energy $E_x \approx$ 15-17 MeV may be of some interest. The underlying nuclear $J = 2^{-}$ level of ^{6}He has mainly $^{33}P_2$ [33] structure and corresponding hypernuclear states should be very narrow ($\Gamma \approx 1.5$ MeV) [20], because they lie just above the threshold of the only opened decay channel ($^{4}He_{\Lambda}^{*} + {}^{4}He$).

In $^{9}Li_{\Lambda}$ (fig 14) the low-spin members of all three spin doublets (ground state and the doublets built on $J = 1^{+}$ E = 0.98 MeV and $J=3^{+}$, E = 2.25 MeV excited states of ^{8}Li) are rather weakly populated in comparison with high-spin ones. However, the triple differential cross sections are measurable and the energy splittings of first and third doublet is predicted to be sufficiently large in all models (≈ 0.2 - 0.3 MeV), so it is measurable with present experiment.. The valuable information on the relative positions of different doublets (and consequently on nucleon spinorbit parameter S_N of ΛN effective interaction) can be obtained in this vay.

The similar situation (only one member of each doublet is strongly populated) is examined for $^{12}B_{\Lambda}$ hypernucleus (Fig. 11). In addition, the ground state doublet is nearly degenerated in all models and unresorvable with energy resolution of few hundredths keV. The additional peaks found in KEK (π^{+}, K^{+}) experiment [12] should be clearly visible in (e,e'K) and the contradiction between the data and weak coupling model predictions might be confirmed or doubt.

The $^{12}B_{\Lambda}$ hypernucleus is extremely bound one, $E_{thr} = 11.37$ MeV. It is supposed, therefore, that some of the positive parity states ($J = 0^{+}$, 1^{+}, 2^{+}, 3^{+}) at $E_x \approx$ 10-11 MeV with (p^{-1}, p_{Λ}) structure may be below the threshold. The $| p_{3/2} (\Lambda) * {}^{11}C (J=3/2^{-}$, gr.st.); $J = 0^{+} \rangle$ state strongly populated in (K^{-}, π^{-}) recoilles reaction at $E_x \approx 10.6$ MeV in mirror $^{12}C_{\Lambda}$ hypernucleus is not populated in (e,e'K^{+}). An unresolved group of $J = 2^{+}$ states in the same energy region was seen in (π^{+}, K^{+}) reaction. Due to the strong spin-flip, also $J = 1^{+}$ and especially $J = 3^{+}$ members of this multiplet may be populated in (e,e'K^{+}) - see Fig. 11. Taking into account the larger binding energy of the mirror $^{12}B_{\Lambda}$ hypernucleus, at least some of these states should be particle stable.

The situation seems to be much better in $^{16}N_\Lambda$ hypernucleus (Fig. 12). Both the members of ground state (built on $J = 1/2^-$ ground state of ^{15}N nucleus) as well as excited state ($J = 3/2^-$, $E = 6.32$ MeV) doublet are populated with sufficient strengths. A careful investigation of ground state doublet can confirm or question commonly accepted assumption of nearly degenerate $^{16}N_\Lambda$ ground state doublet [8,11].

In high resolution (e, e'K^+) it will be also possible to obtain an interesting spectroscopic information from the positions and escape widths of some 1 hω hypernuclear states (p^{-1}, p_Λ) and (s^{-1}, s_Λ) in some cases). This states are particle unstable as a rule (with already mentioned exception of $^{12}B_\Lambda$), but the estimated escape widths of many of them are rather small, few tens keV to 1 MeV [11]. A typical example is a $J = (3/2^-,5/2^-)$ doublet at $Ex \approx 15$ - 17 MeV in $^{7}He_\Lambda$ with estimated widths $\Gamma \approx 2$ MeV [20]. The lower member $J = 3/2^-$ of the doublet is well seen in (K^-, π^-) reaction on ^{7}Li [20]. In (e, e'K^+) reaction both the members of the doublet should be populated (Fig. 13).

The estimated widths of some particle unstable states in the second half of the 1p shell may be very small. It is predicted e.g. that some $J = 2^+$ states in $^{16}O_\Lambda$ ($^{16}N_\Lambda$) at excitation energy approximately 10 -15 MeV will be as small as $\Gamma \approx 15$ - 40 keV, instead of the fact that $E_{thr} = 6.9$ MeV only for $^{16}O_\Lambda$. The states of this type in mirror $^{16}N_\Lambda$ hypernucleus are also distinguishable in (e, e'K^+) - Fig. 12. Careful investigation of the position and especially of width of these states may serve as a valuable check of hypernuclear wave functions and decay mechanism.

4. Kinematical conditions and counting rates

The kinematical and experimental conditions for (e, e'k) experiments on ^{7}Li, ^{9}Be, ^{12}C and ^{16}O targets are reported in table I, where the values for solida angles come from the new proposed setup thet includes two septa (see Appendix A) They are the same for all the measurements performed on the different targets.

The luminosity, obtained with constant beam current of 100 μA and target thickness of 100 mg/cm^2 ranges from 2.4×10^{36} to 5.4×10^{36}

The single events and accidental coincidences counting rates result to be quite constant for all the investigated nuclei and the numbers reported in table II represent upper limits in our conditions.

The single electron arm counting rates are computed with the QFS code of Lightbody and O'Connel [22] with the added contribution of the elastic radiative tail which gives electron elastically scattered into the spectrometer after having loss the right energy through bremsstrahlung emission of real photons in the target. This contribution has been estimated by means of the approximated formula C.11 of ref.[23]

The kaon rate is estimated following the procedures suggested in ref. [24]. The accidental rates are calculated considering a time coincidence resolution of 1 ns and a duty cicle of 100% .

Cross sections, calculated as specified in the previous chapter, and expected counting rates for different hypernuclear levels populated in $^{7}Li(e,e'K)^{7}He_{\Lambda}$, $^{9}Be(e,e'k)^{9}Li_{\Lambda}$, $^{12}C(e,e'k)^{12}B_{\Lambda}$ and $^{16}O(e,e'k)^{16}N_{\Lambda}$ experiments are reported in tables IIIa-b.

Table I

Kinematical conditions

E_i (GeV)	4
E_o (GeV)	1.8
Θe (°)	6
$\Delta E/E$ (%)	± 5
$\Delta\Omega_e$ (msr)	4.5
p_k (GeV)	1.96
$\Delta p/p$ (%)	± 5
Θ_k (°)	6
$\Delta\Omega_k$ (msr)	4.5
N_e	$6.2x10^{24}$
target thickness (mg/cm2)	100
K surv. prob. (%)	18

TABLE II

Single and accidental rates

(e,e') single rate (s^{-1})	$1.17x10^{5}$
(e,k) single rate (s^{-1})	$3.6x10^{2}$
(e,p) single rate (s^{-1})	$1.8x10^{5}$
(e,π) single rate (s^{-1})	$2.9x10^{3}$
(e,e'k) accidental rate ($hour^{-1}$)	0.96 (300 keV bin) 0.19 (300 keV bin, split target) (5 x 20 mg/cm^2)

Tab.III a $^{7}Li(e,e'K)^{7}He_{\Lambda}$ and $^{9}Be(e,e'k)^{9}Li_{\Lambda}$ cross sections and counting rates

	E MeV	*J*	*(e,e'K) nb/GeV/sr²*	*Rate hr-1*
^{7}Li (e,e'K)	0.0	1/2+	0.796	10.2
	1.59	5/2+	0.181	2.3
	1.94	3/2+	0.138	1.7
	15.46	3/2-	0.345	4.25
	17.67	3/2-	1.14	14.6
$^{9}Be(e,e'K)$	0.0	3/2+	0.179	1.78
	0.69	5/2+	0.975	9.7
	1.42	1/2+	0.196	1.95
	1.71	3/2+	0.282	2.8
	2.43	5/2+	0.108	1.07
	2.78	7/2+	0.306	3.04

Tab.3 b $^{12}C(e,e'k)^{12}B_{\Lambda}$ and $^{6}O(e,e'k)^{16}N_{\Lambda}$. cross sections and counting rates

	E MeV	*J*	*(e,e'K) nb/GeV/sr²*	*Rate hr-1*
$^{12}C(e,e'K)$	0.0	1-	0.789	5.89
	0.03	2-	4.57	34.6
	2.54	1-	2.0	14.9
	5.46	2-	0.599	4.47
	6.05	3+	0.12	0.98
	10.03	3+	0.778	5.81
	10.63	3+	3.58	27.1
	11.22	2+	0.609	4.54
	11.93	2+	0.293	2.18
$^{16}O(e,e'K)$	0.0	1-	2.78	20.7
	0.44	0-	0.26	1.91
	6.89	1-	2.01	15
	7.03	2-	5.28	39.4

The absolute cross sections will also be measured with high accuracy and compared with the elementary process on proton in order to extract information on nuclear-hypernuclear transition. Measurements on hydrogen will be done taking advantage of the waterfall target we will use for the Oxygen [25].

In fact the missing mass spectrum at given kinematics (Ee= 4 GeV, Ee'=1.8 GeV) for $^{16}N_{\Lambda}$

production consists of two peaks: ground state doublet peak at M=176.5 MeV ($\approx m_\Lambda - m_p$)because the binding energy of Λ in $^{16}N_\Lambda$ and binding energy of p in $^{16}O_\Lambda$ are almost the same by chance) and another at M = 183.5 MeV corresponding to the doublet of excited states at Ex = 7 MeV. For e + p ===> e' + k + Λ (Σ) corresponding peaks lie at M = 177.4 MeV ($m_\Lambda - m_p$) and M = 254 MeV (= $m_\Lambda - m_p$) .. " Misinterpreted" missing mass spectrum would consist of peak at M = 147.8 MeV (kaon from ^{16}O interpreted as kaon from proton target) and M=213.1 MeV (kaon from proton target interpreted as kaon from ^{16}N production). They are far enough from true peaks due to the large difference in recoil momenta of produced $^{16}N_\Lambda$ and Λ hyperon ($m_k/m\Lambda$ ~1/2, $m_k/M^{12}N_\Lambda$~1/30).

5. Detector Performances

For both the HRS's spectrometers of the Hall A experimental equipment, the forward scattering angles capability is considered with the use of two septum magnets (see appendix A).

With the properties of the CEBAF electron beam and the considered spectrometers, the level of 280 KeV in energy resolution could be achieved in (e,e'k) experiments with thin targets. In our case the targets proposed have thickness of 100 mg/cm^2. In this case they are not thin enough to reach the required resolution due to the spread in energy caused by the energy loss in the target which depends on the interaction point. To obtain a better resolution, it is possible to split the target in several thinner targets (see fig. 15) with the optical properties of the spectrometer allowing the identification of the source target point and hence the eventual correction for the known energy loss in the crossed targets other than that from where the kaon is knocked-out.

An example of the gain in resolution with this method can be seen in figures 16a and 16b. Fig.16a shows a Monte Carlo simulation of the momentum spread distribution for a kaon produced with a momentum of 1.5 GeV/c at the vertex of interaction in a ^{12}C target of 100mg/cm^2. Fig. 16b shows the spread when the kaon is produced in the third layer out of five identical subsequent layers with a thickness of 20 mg/cm^2 with the inclusion of the straggling caused by the two subsequent layers. While in the first case a spread of about 150 KeV/c is obtained, giving a big contribution to the resolution, in the second case one has a spread of about 40 KeV/c that allows to reach the required resolution. The shift in momentum is due to the energy loss in the fourth and fifth target and it is a calculable quantity.

Moreover a segmented target allows to reduce the accidental coincidence rate if the origin from the same target is imposed to the electron and kaon detected in coincidence.

In this scheme the contribution to the resolution of the primary electron beam is important and, to achieve a 280 keV resolution, the primary beam must be dispersed on the target and the double dispersion matching technique has to be used.

Table IV

Energy resolution assuming a momentum dispersed beam

Source		*Error*
primary beam	($2x10^{-4}$ of 4 GeV)	80 keV
outgoing electron	(10^{-4} of 1.8 GeV)	180 keV
outgoing kaon	(10^{-4} of 1.96 GeV)	190 KeV
kaon straggling on split target	40 KeV	40 keV
Total		280 keV

The particle identification will be made by means of the standard HRS detector package. In the electron arm time-of-flight, gas and aerogel Cerenkov counters and shower counters allows to distinguish e^- from π^- and K^- with a rejection ratio $\geq 10^5$. In the hadron arm, kaons will be separated from pion by TOF and aerogel and from protons by TOF with the needed rejection ratio. Standalone kaon separation from proton is also possible, if needed, by moving the aerogel cerenkov detector from the electron arm and substituting it with aerogel of different refractive index (1.06 instead of 1.025).

6. Beam time requests

According to the (e,e'k) coincidence event rates reported in Tables III, the less populated levels in which we are interested give about a contribution from ≈ 2 to ≈ 40 counts/hour to the total counting. The accidental counting rate ranges from a factor ≈ 10 to ≈ 100 less, then it does not influence the statistical accuracy in a substantial way.

With 120 hours of beam time per nucleus (^{12}C, ^{16}O, ^{7}Li and ^{9}Be) a statistical accuracy from ≈ 2 to ≈ 5 % is achieved for the most important levels. Adding 100 hours (≈ 20%) of beam time to take into account calibration and contingency, we think that with 580 hours of beam time a first complete study of high resolution hypernuclear spectroscopy in p shell nuclei can be accomplished.

References

[1] G. Alexander et al.:Phys. Rev. 173 (1968) 1452

[2] J. Pniewski et al.: Nucl. Phys. A443 (1985) 685

[3] H. Bando, T. Motoba, M. Sotona, and J. Zofka: Phys. Rev. C39 (1989) 587

[4] A. Gal, J. M. Soper, and R. H. Dalitz: Ann. Phys. (N.Y.) 63 (1971) 53;

[5] R. H. Dalitz and A. Gal: Ann. Phys. (N.Y.) 116 (1978) 167

[6] M. Bedjidian et al.: Phys. Lett. 83B (1979) 252

[7] M. May et al.: Phys. Rev. Lett. 51 (1983) 2085

[8] D. J. Millener, A. Gal, C. B. Dover, and R. H. Dalitz:
Phys. Rev. C31 (1985) 499

[9] R. E. Chrien: Czech. J. Phys. B39 (1989) 914;
Nuovo Cim. 102A (1989) 727

[10] R. E. Chrien et al.: Phys. Rev. C41 (1990) 1082

[11] V. N. Fetisov, L. Majling, J. Zofka, and R. A. Eramzhyan:
Z. Phys. A339 (1991) 399
preprint 102, Lebedev Phys. Inst., Moscow 1990

[12] T. Hasegawa et al.: Core excited states of 12CΛ hypernuclei formed in the (π+,K+) reaction, INS-Rep.-1037, University of Tokyo, 1994

[13] Y.Yamamoto et al.: Czech. J. Phys. 42(1992)1249

[14] M. Sotona, and S. Frullani; submitted to Prog. Theor. Phys.

[15] B.R. Martin: Nucl. Phys. B94(1975)413

[16] K. Itonaga, T.Motoba, O.Richter and M. Sotona: Phys. Rev. C49(1994) 1045

[17] R. A. Williams, Ch.-R. Ji, and S. R. Cotanch:
Phys. Rev. C46 (1992) 1617

[18] A. G. M. van Hees and P. W. M. Glaudemans:
Z. Phys. A314 (1983) 323

[19] R. A. Williams, Ch.-R. Ji, and S. R. Cotanch:
Phys. Rev. D41 (1990) 1149

[20] O. Richter, M. Sotona, J. Zofka: Phys. Rev. C43 (1991) 2753

[21] S.Frullani, F.Garibaldi, F.Ghio, M.Jodice, G.M.Urciuoli, R.De Leo, Multi Purpose Spectrometer, I.N.F.N. - I.S.S. 90/5, July 1990

[22] J.W.Lightbody Jr., J.S.O'Connel, Comp.in Physics, May/June 1988, p.57

[23] L.W.Mo and Y.S.Tsai, Rev. Mod. Phys. 41(1969)205

[24] C.E. Hyde-Wright, W.Bertozzi, J.M.Finn Proc. of the 1985 CEBAF Workshop

[25] F. Garibaldi et al. NIM A314 (1992) 1-8

Figure captions

Fig. 1. Strength functions for (K^-,π^-), (π^+,K^+) and (e,e'K^+) reactions on ^{12}C target

Fig. 2. Predicted energy spectra of $^7He_\Lambda$

Fig. 3. Predicted energy spectra of $^9Li_\Lambda$

Fig. 4. Predicted energy spectra of $^{12}B_\Lambda$

Fig. 5. Predicted energy spectra of $^{16}N_\Lambda$

Fig. 6. Correspondence of the ^{11}C energy levels and observed $^{12}C_\Lambda$ hypernuclear states .

Fig. 7. DWIA description of hypernuclear cross sections in (π^+,K^+) reaction.

Fig. 8. $p(\gamma,K^+)\Lambda$ photoproduction cross section comparred with LC4 model predictions (solid line).

Fig. 9. Electroproduction invariant cross section σ_{UL} as a function of q^2. LC4 model - solid curve.

Fig. 10. The dependence of the $^{12}C(e,e'K^+)^{12}B_\Lambda$ cross section on the energy E_γ of virtual photon for $J=2^-$, E=7.03 MeV state of $^{16}N_\Lambda$,E'_e = 1.3 GeV, $\Theta_e=7^o$ and $\Theta_K = \Theta_\gamma$.

Fig. 11. Predicted strength function for $^7Li(e,e'K^+)^7He_\Lambda$ reaction with LC4 elementary amplitude. E_e = 4 GeV, $E_{e'}$ = 1.8 GeV, $\Theta_e = 6^o$ and $\Theta_K=6^o$.

Fig. 12. The same as in Fig. 11 for $^9Be(e,e'K^+)^9Li_\Lambda$

Fig. 13. The same as in Fig. 11 for $^{12}C(e,e'K^+)^{12}B_\Lambda$

Fig. 14. The same as in Fig. 11 for $^{16}O(e,e'K^+)^{16}N_\Lambda$

Fig. 15. Entire and splitted target arrangements

Fig. 16.a),b) Monte Carlo simulation of the measured momentum spread distribution for a kaon of 1.5 GeV/c at the interaction point: a) in the case of entire target of 100mg/cm2; b) in the case of segmented target (5x20mg/cm2)

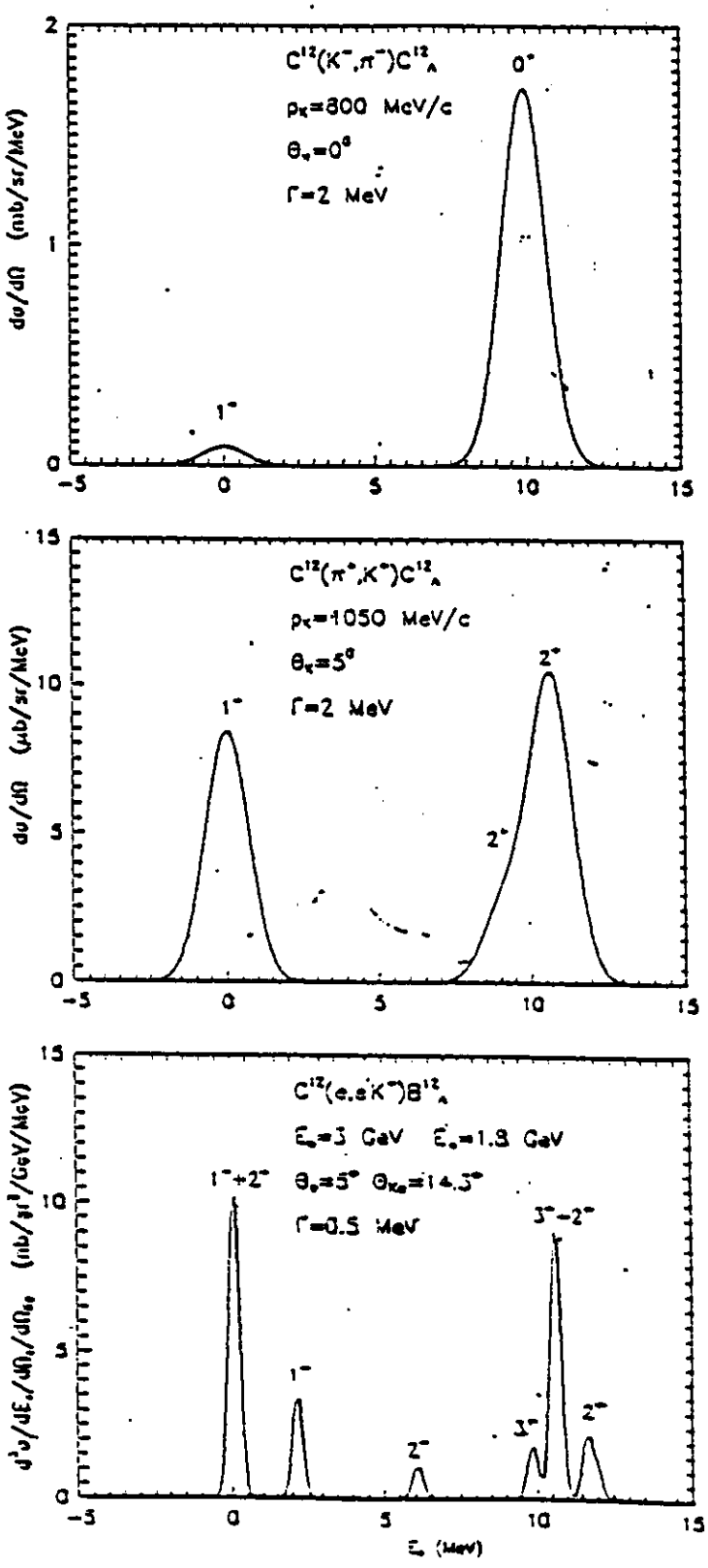
$C^{12}(K^-,\pi^-)C^{12}_\Lambda$
p_K=800 MeV/c
θ_π=0°
Γ=2 MeV
0⁺
1⁻
dσ/dΩ (mb/sr/MeV)
$C^{12}(\pi^+,K^+)C^{12}_\Lambda$
p_π=1050 MeV/c
θ_K=5°
Γ=2 MeV
1⁻
2⁺
2⁺
dσ/dΩ (μb/sr/MeV)
$C^{12}(e,e'K^+)B^{12}_\Lambda$
E_e=3 GeV E'_e=1.8 GeV
θ_e=5° θ_{K^+}=14.3°
Γ=0.5 MeV
1⁻+2⁻
1⁻
2⁻
3⁻-2⁻
3⁻
2⁻
E_Λ (MeV)

Figure 1

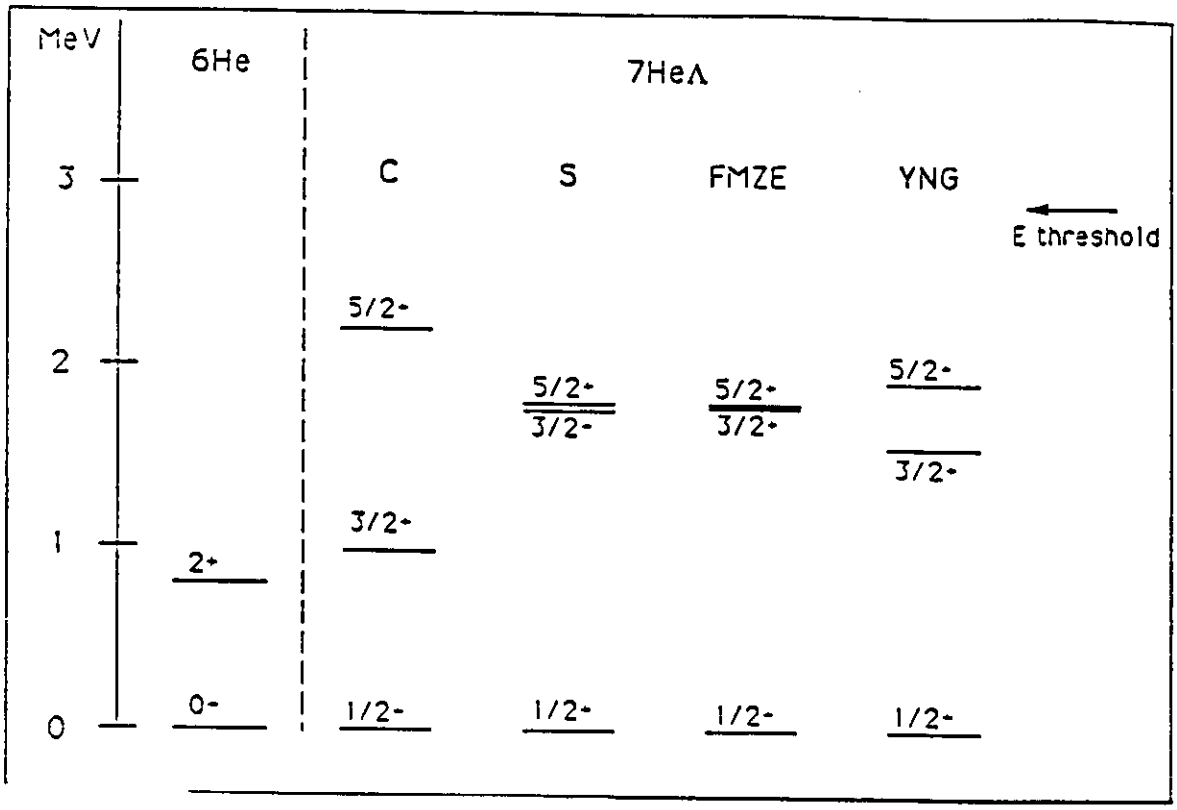

Figure 2

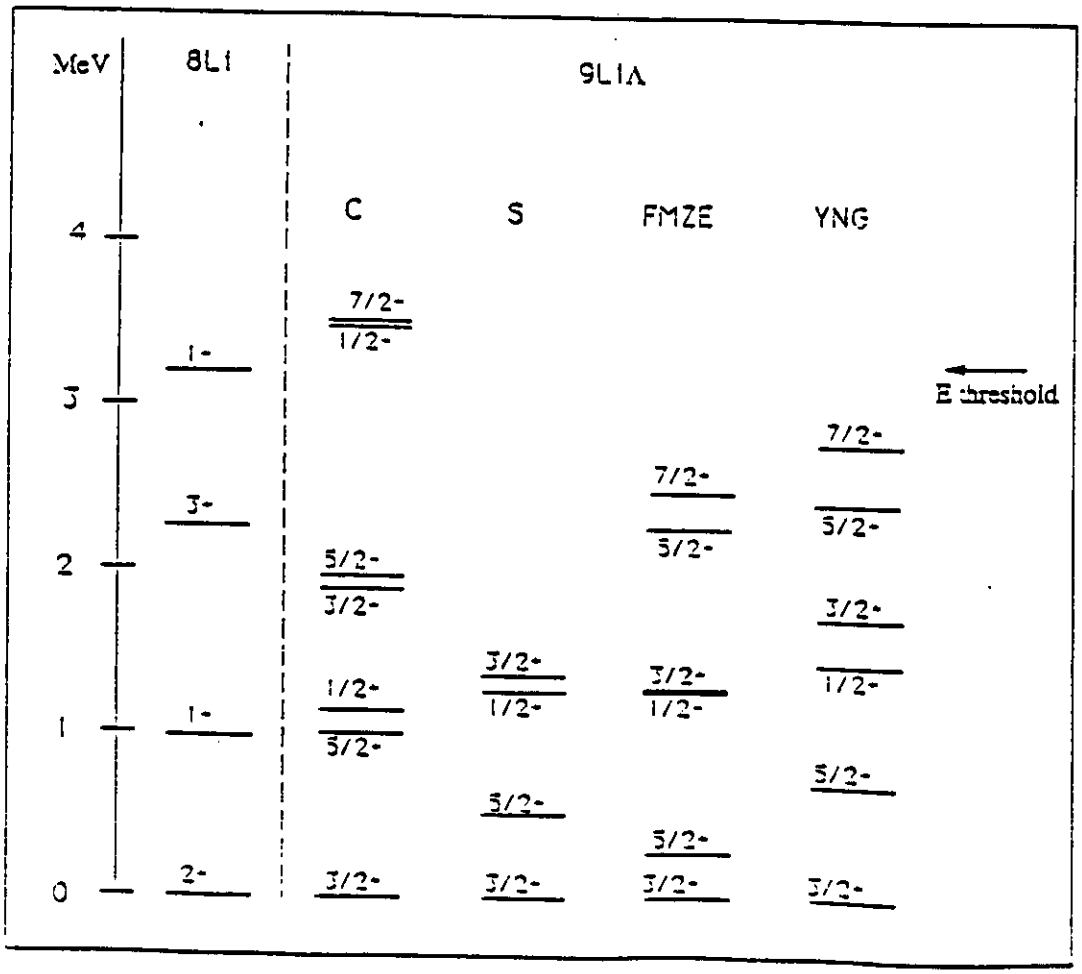

Figure 3

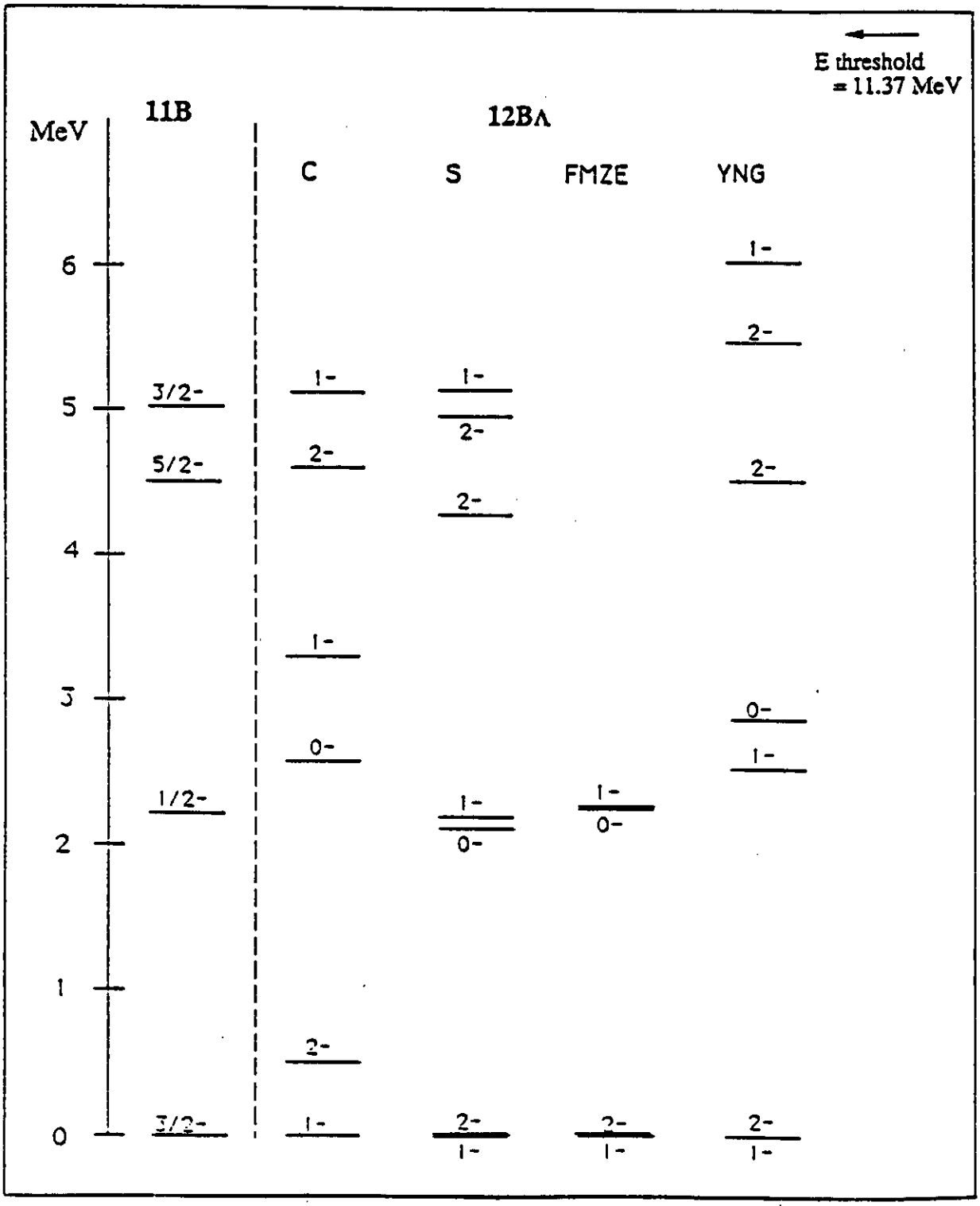
E threshold
= 11.37 MeV
MeV
11B
12BΛ
C
S
FMZE
YNG
6
5
4
3
2
1
0
3/2-
5/2-
1/2-
3/2-
1-
2-
1-
0-
2-
1-
1-
2-
2-
1-
2-
1-
0-
1-
0-
2-
1-
2-
1-
1-
2-
0-
1-
2-
1-

Figure 4

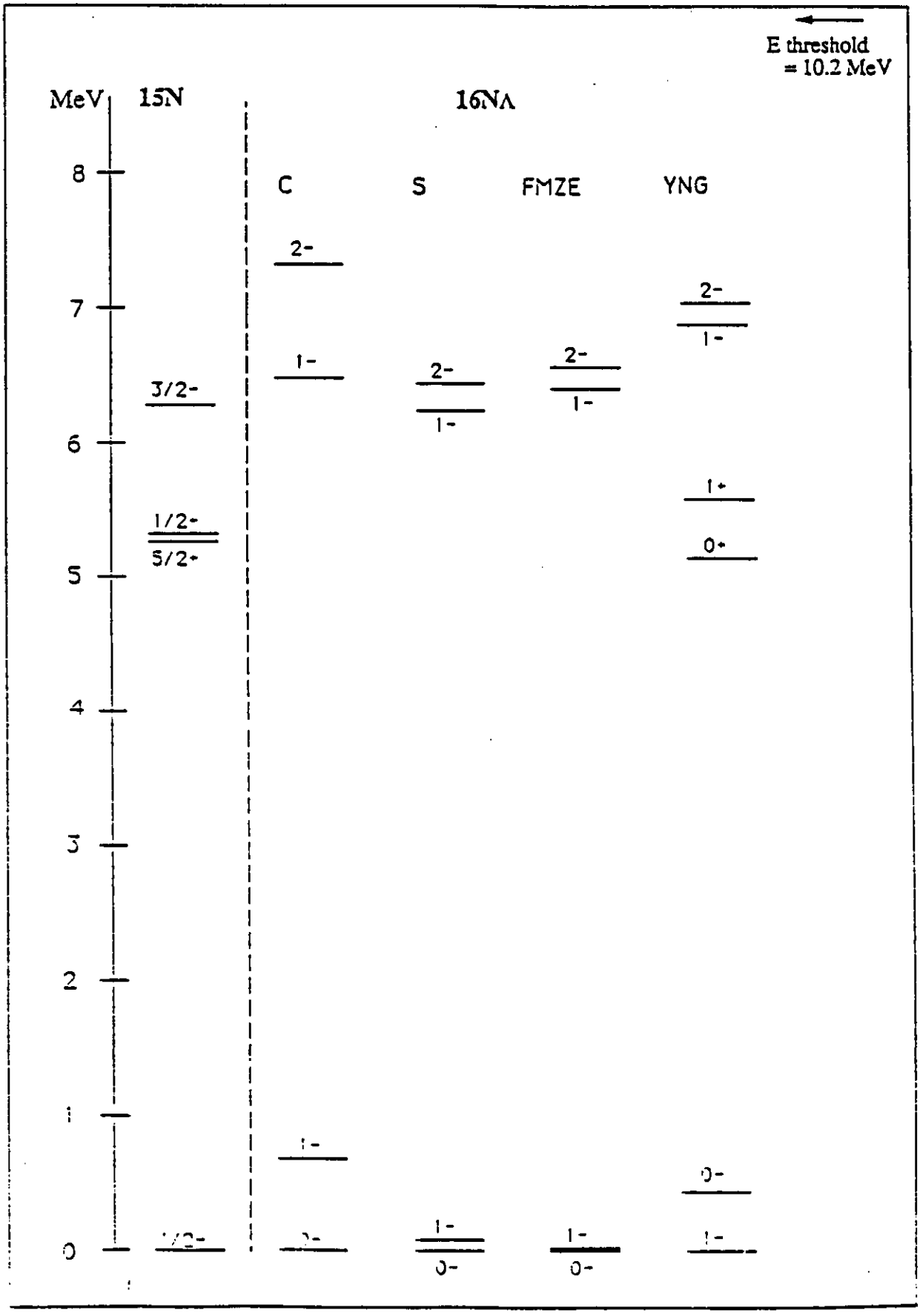
E threshold
= 10.2 MeV
MeV
15N
16NΛ
C
S
FMZE
YNG
8
7
6
5
4
3
2
1
0
3/2-
1/2-
5/2+
2-
1-
2-
1-
2-
1-
2-
1-
1+
0+
1-
0-
1-
0-
1-
0-
1-
0-

Figure 5

$^{12}C(\pi^+,K^+)^{12}_{\Lambda}C$, $p_\pi = 1.06$ GeV/c

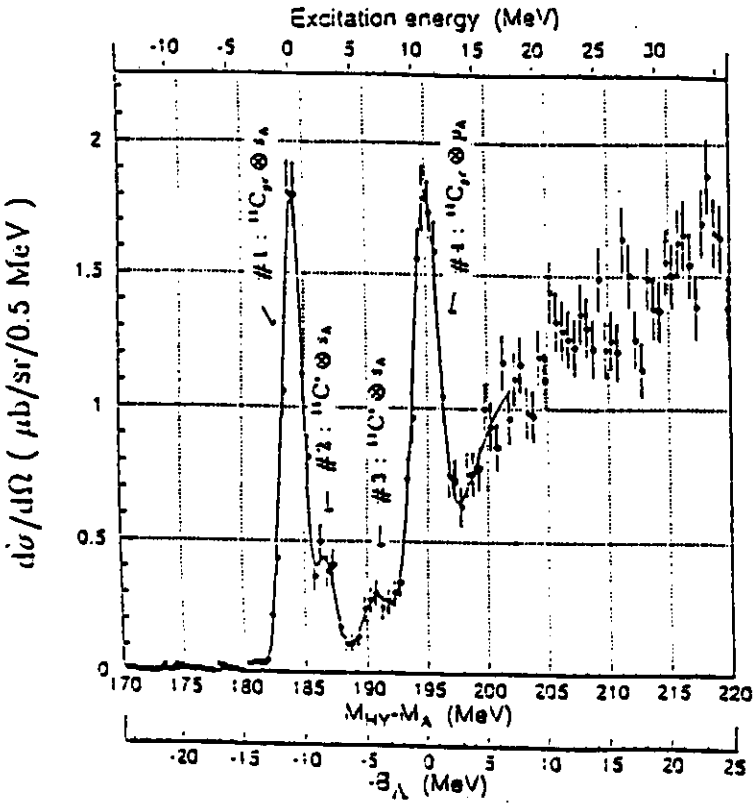

Figure 6 a

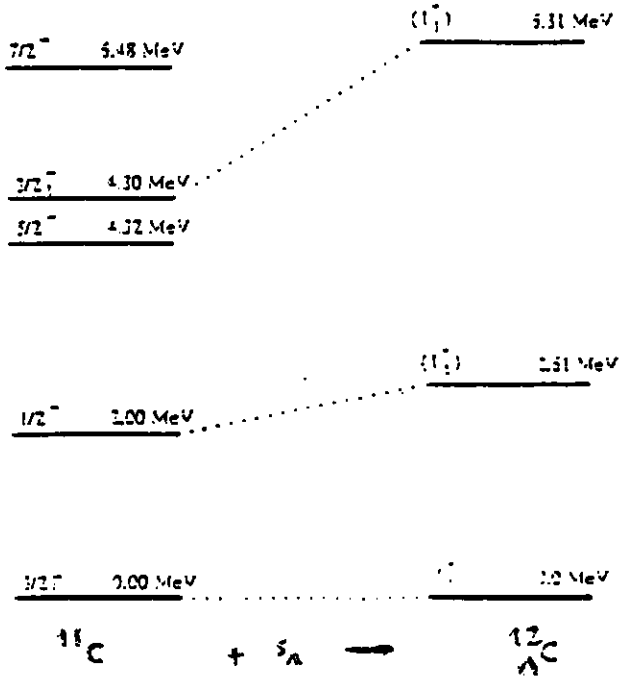

Figure 6 b

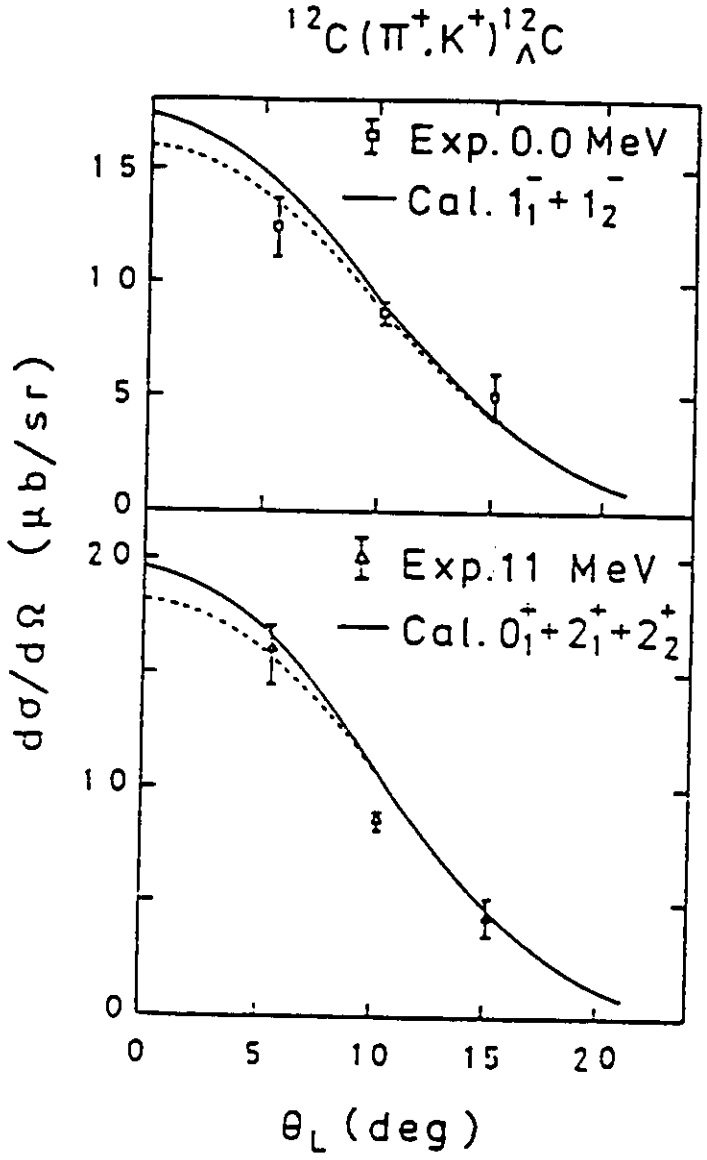
$^{12}C(\pi^+,K^+)^{12}_{\Lambda}C$
Exp. 0.0 MeV
Cal. $1_1^- + 1_2^-$
Exp. 11 MeV
Cal. $0_1^+ + 2_1^+ + 2_2^+$
$d\sigma/d\Omega$ (μb/sr)
θ_L (deg)
0
5
10
15
20

Figure 7

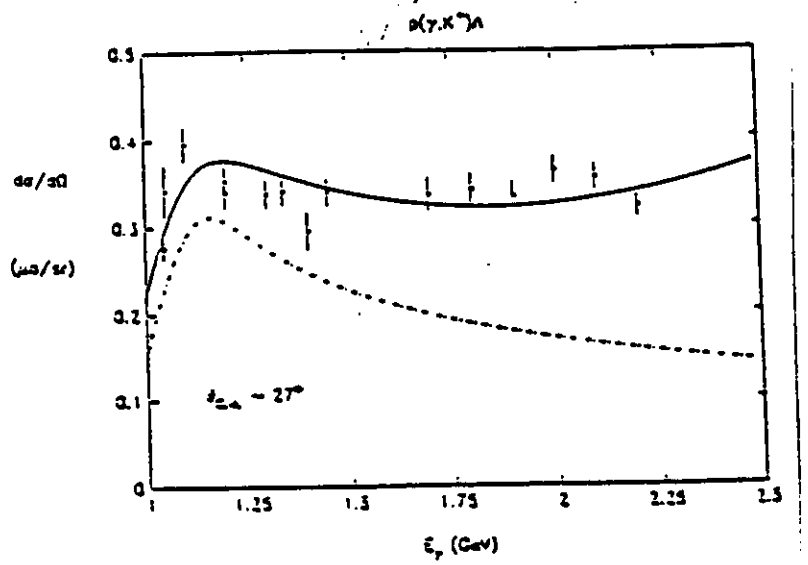

Figure 8

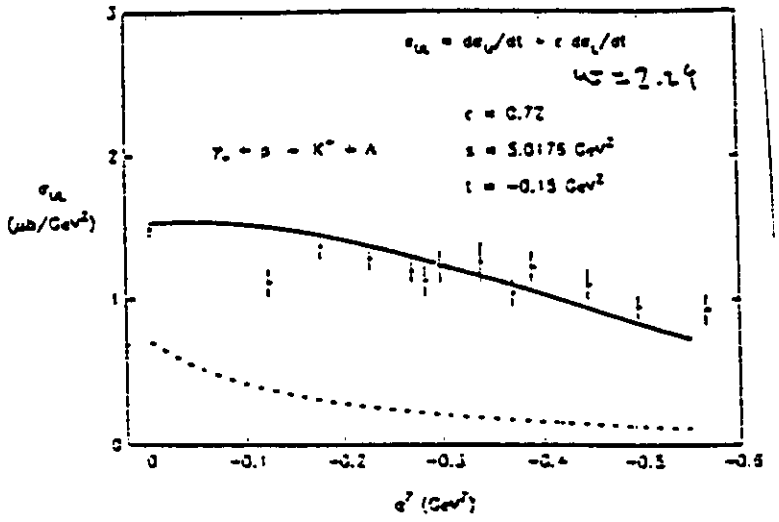

Figure 9

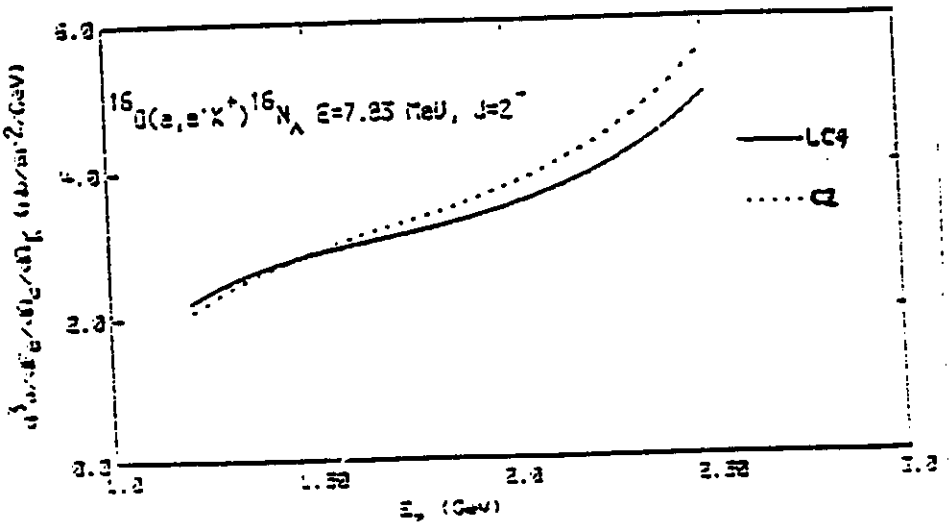

Figure 10

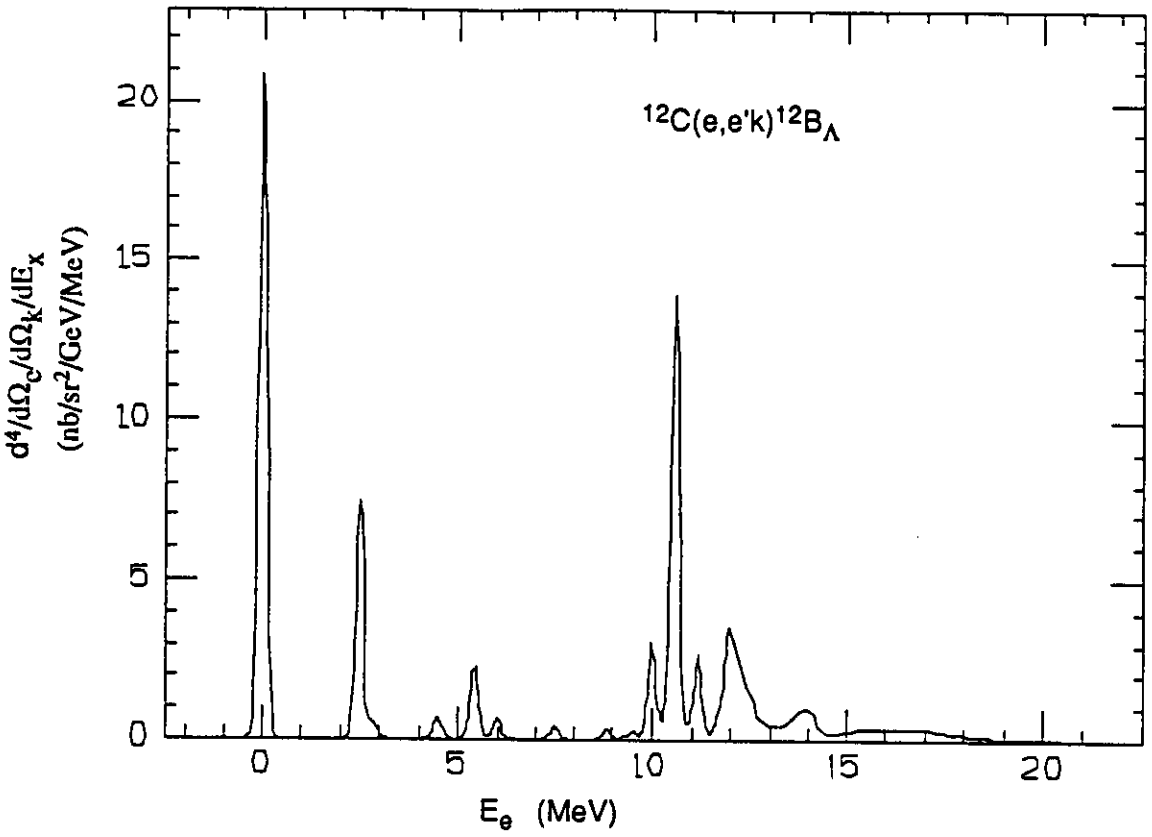

Figure 11

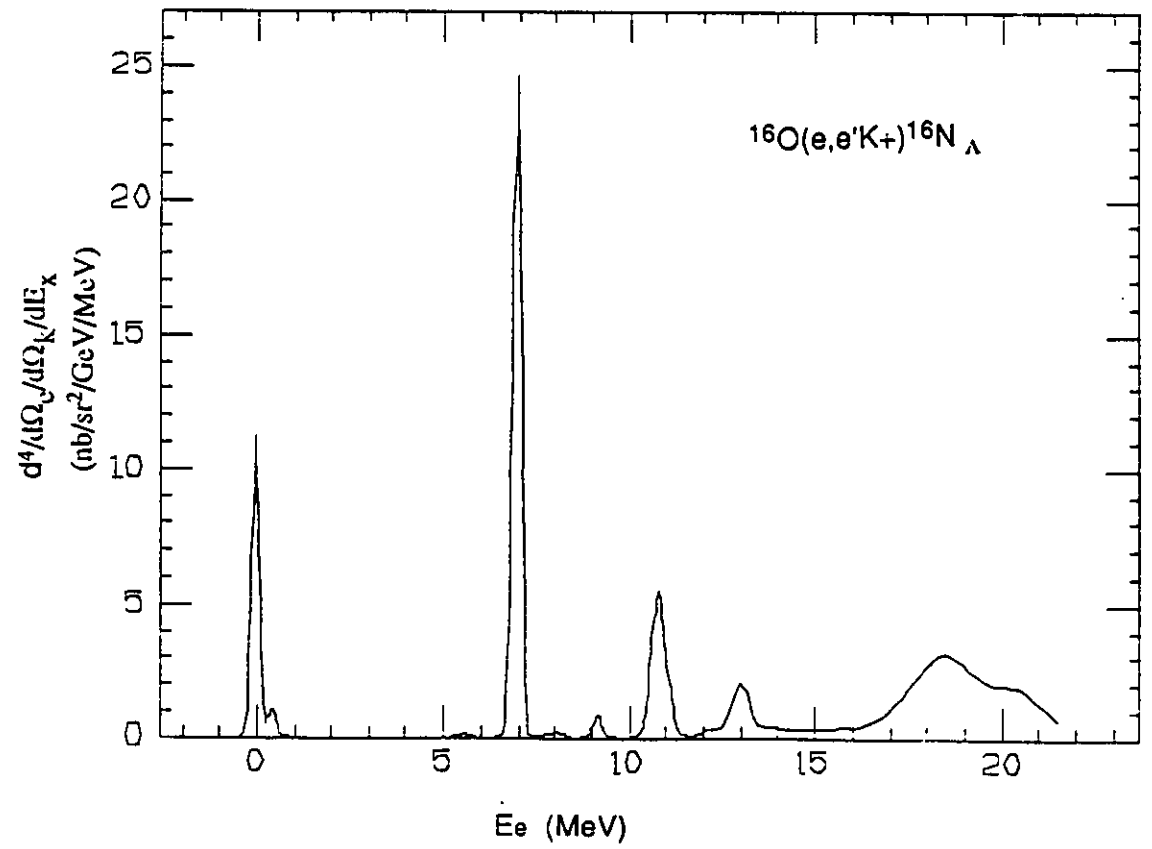

Figure 12

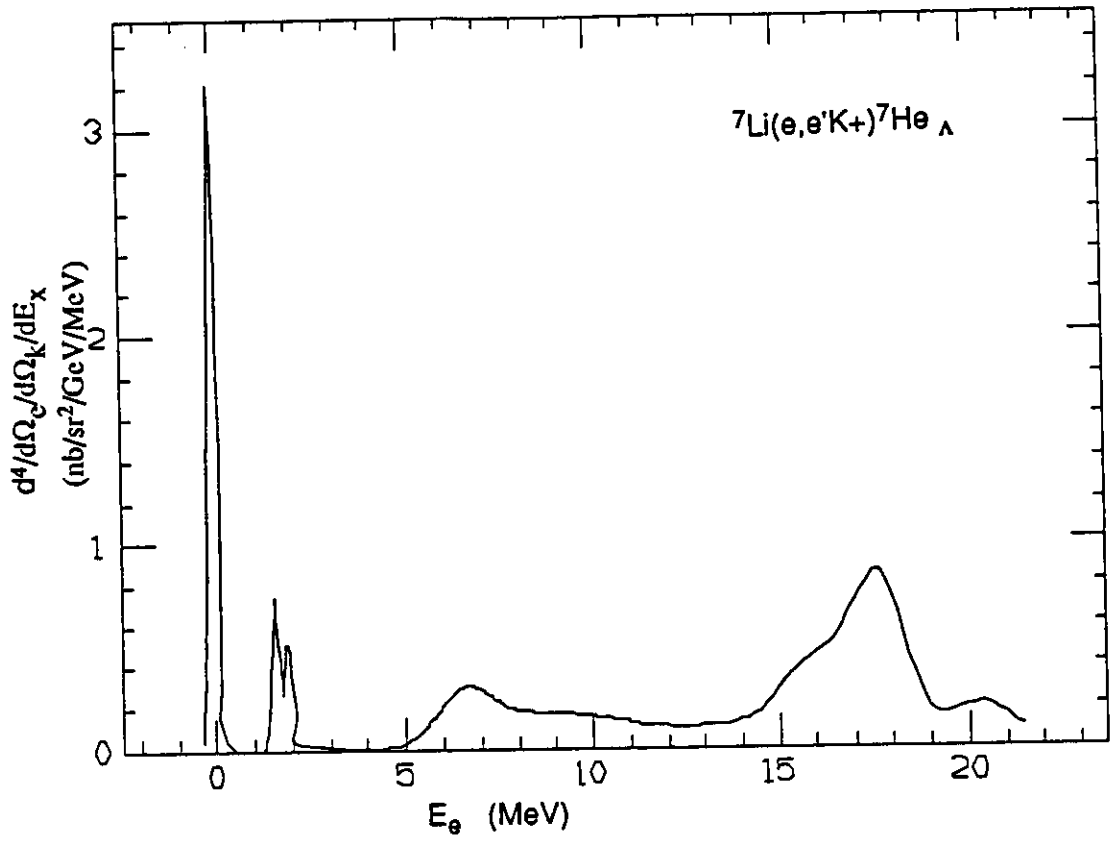

Figure 13

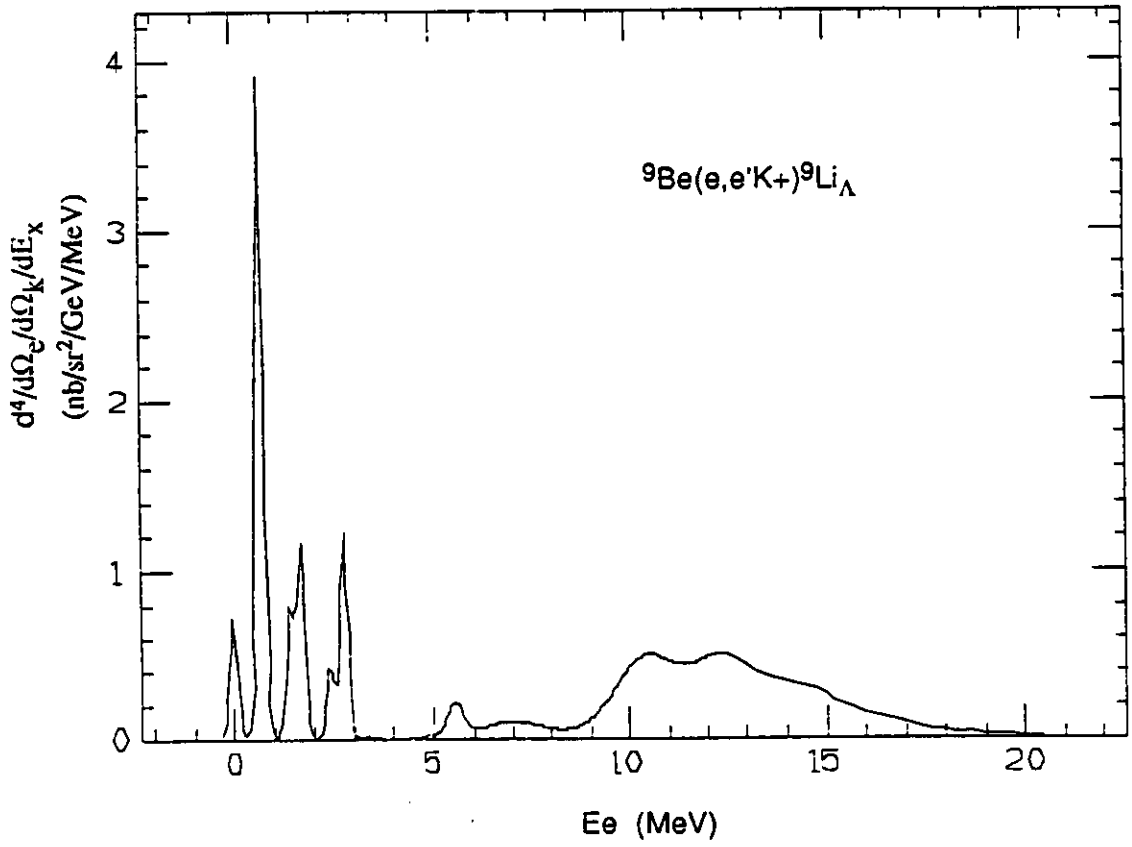

Figure 14

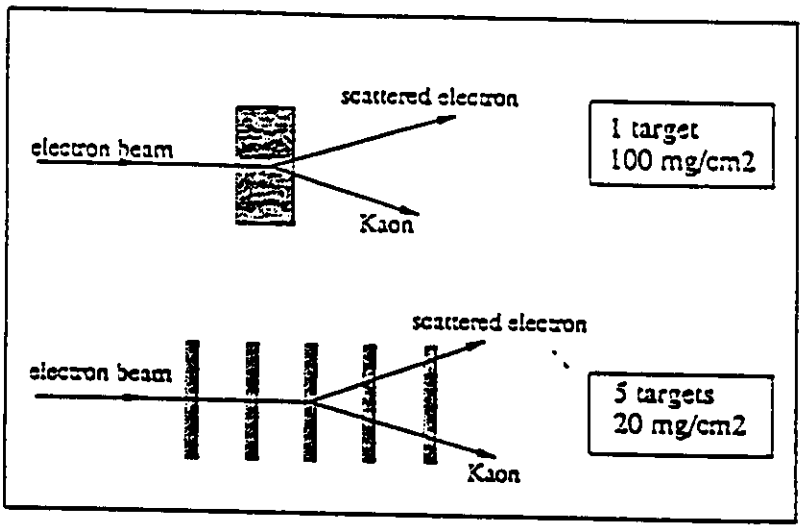

Figure 15

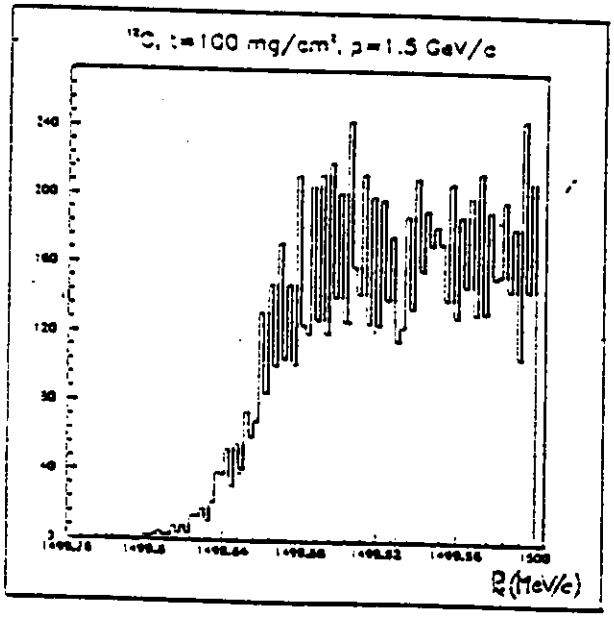

Fig. 16a

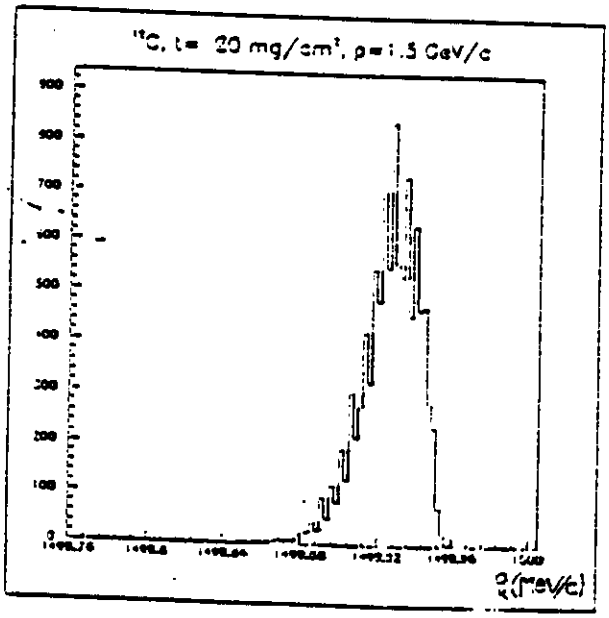

Fig. 16b

- APPENDIX A -

- Septum Magntes for CEBAF Hall A

Septum magnets are needed for the HRS[2] Spectrometers in Hall A at CEBAF to allow experiments using scattering angles smaller than the minimum angle of 12.5° (or about 10° if the front quadrupole doublet is moved back).

The new minimum scattering angle should be about 5°. The idea is to move the target upstream a suitable distance and to insert a horizontal septum magnet before the point element in the spectrometers in such a way that the target seem to be situated on the optical axis of the spectrometers. This is of course true only for the central momentum of the spectrometer, for other momenta the target will appear to be displayed sideways.

The septum magnets should change the particle orbit by about 7.5°. The length of the septum is determined by the particle momentum and the field B in the septum according to

$$L = 0.5822 \frac{p(GeV/c)}{B(kG)} \beta(^{\circ})$$

where β is the angle of bend for the septum. For $\beta = 7.5^{\circ}$ we get for L (m)

	B (kG)				
p (GeV/c	10	15	20	25	30
1	0.437	0.291	0.218	0.175	0.145
2	0.874	0.583	0.487	0.349	0.291
3	1.311	0.874	0.655	0.524	0.437
4	1.748	1.165	0.874	0.699	0.582

Tab 1: Septum length in meters as function of the particle momentum p and the septum magnetic field B

We must also calculate where the septum should be placed to be able to calculate the drift distance etc. The situation is shown in Fig. 1. where the z-axis is the beam line, z=0 the "standard" target position and the new target position is moved a distance Z_{eff} upstream. Φ is the particle scattering angle and β the septum angle.

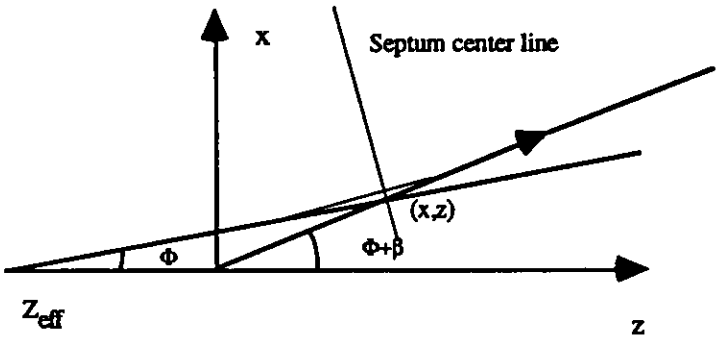

Fig. 1 Position of the septum center line

The two lines

$$x = \tan(\phi) \bullet (z + z_{eff})$$
$$x = \tan(\phi + \beta) \bullet z$$

must be tangent to the circular orbit through the septum, and the center of the septum must be on the dotted line in fig 1. The point (x,z) where the tangents cross each other, has the cordinates

$$x = \frac{\tan(\phi) \bullet \tan(\phi + \beta)}{\tan(\phi + \beta) - \tan(\phi)} \bullet z_{eff}$$
$$z = \frac{\tan(\phi)}{\tan(\phi + \beta) - \tan(\phi)} \bullet z_{eff}$$

and the distance from the displaced target position to x,z is

$$D = \sqrt{(z + z_{eff})^2 + x^2} = z_{eff} \frac{\tan(\Phi + \beta)}{(\tan(\Phi + \beta) - \tan(\Phi)\cos\Phi}$$

We notice that D is a function of Φ and β for a fixed z_{eff}, which means the septum must be movable in the longitudinal direction if it is to be used for different scattering angless if β is fixed. The magnitude of the longitudinal motion depend on β, the larger the β the less longitudinal motion.

To get the most flexible arrangement we need to separate the septum magnet for each spectrometer. This allows each spectrometer to operate at different scattering angles, momenta and polarity.

The HRS^2 spectrometers uses superconducting technology, so, first of all, we have tried to see if it is possible to make also the septum in form of superconducting cosinus dipole

We have to make some layout to get an idea about possible limitations. The HRS^2 front end is

Drift distance Target - Q1	1.69 m
Angular acceptance, horizontal	± 30 mrad
vertical	± 65 mrad

We move the target 0.8 m upstream, and we further assume we can get up the 30 kG field in the septum magnet that we want to handle with momenta of 3 GeV/c. Furthermore we assume the dump line after the target is conical with an opening angle of ±1.5°.

In the first layout, shown in Fig. 2, the scattering angle is 5° and the septum, assumed to have a field of 3 T, is bending 7.5°. In the bottom part of the figure is a horizontal view of the region between the target and Q1 and in the upper part of the figure is a cross scetion of the septum magnet with the apertures needed at the exit and at the entrance drawn in and also the exit beam line at the septum with a useful bore radius of 100 mm, and the beam is displaced as far as possible towards the edge of the used bore. However, we notice we only have 35 mm space for vacuum chamber, coils and cryostat, which probably is not enough.

In Figure 3 the scattering angle is increased to 6° but β is still 7.5 °. We now have 55 mm for the vacuum chambers, coils and cryostat which is more reasonable. Thus, using just one superconducting septum magnet, a minimum scattering angle of 6 - 6.5 ° can be reached. In the layout we have used a septum field of 3 T but it can be lower, 2.5 T for example.

For larger scattering angles the septum magnet moves back further, and the size of the beam apertures grows.

However, if we really want to measure 5°, we must think about something different, and one way out is to use a room temperature septum in front of the superconducting one. Such a layout is shown in Fig 4, where a room temperature septum with a 2° angle of bend and a field of 1 T is placed in front of the superconducting septu magnet. As can be seen the septum magnet in Fig. 3 can now be used.A cross section of the room temperature septum is shown in Fig. 5. The weight is estimated to less than 160 Kg. This septum is needed only for scattering angles less than 6°, and the idea is to make the vacuum chamber wide enough so the beam can pass through the septum also when there is no field.

Another important question is the maximum scattering angle where the septum magnets can be used. On page A2 we see that this question depends on β and how much free spece there is up to Q1. At 3 GeV/c the maximum scattering angle is 10° -11°, and it increases for low momentum as β x p/B is a constant for the septum magnets see page 1. Thus, to get the largest possible scattering angle the septum magnet should be as strong as possible.

We have also done some calculations to see if we can increase the vertical angular aceptance to compensate for the increased drift distance target-Q1 and, at the same time, use a normal conducting septum magnet.

The result is shown schematically in the Fig.6 The minimum scattering angle is 6° and the septum bends the beam 6.5°. The target is moved forward 0.8 m as in the previous case.

To get the vertical focussing we use a field index n = 10, and also shim angles of 30 degrees at septum entrance and exit to further increase the vertical focussing. The magnetic field in the middle of the magnet is is 1.T, and it increases to 1.75 T for the ray with the largest scattering angle. The vertical angular acceptance is now increased from ± 40 mrad to ± 50 mrad when used at the smallest scattering angle of 6 degrees. The solid angle is now 4.5 msr. For larger scattering angles the vertical angular acceptance decreases as the septum magnet moves further from the target.

The width of the septum is reasonable for a minimum scattering angle of 6° as shown in Fig 6 and the coils can be made as saddle coils, which makes them cheaper. The weight of the septum magnet is about 1.5 tons.

Also in this case it seems that there is no limitation going to angles like 10° - 11° for momenta up to 2 GeV/c.

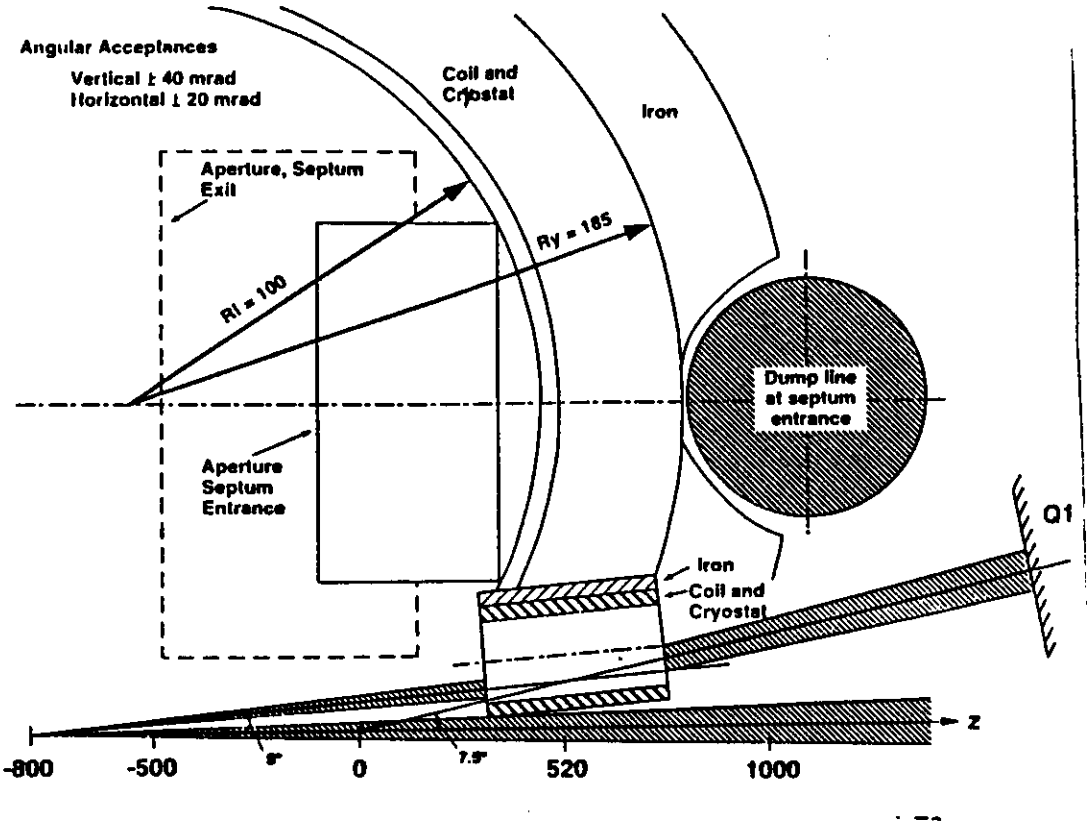

Figure 2 One superconducting Septum $\Phi = 5^\circ$, $\beta = 7.5^\circ$

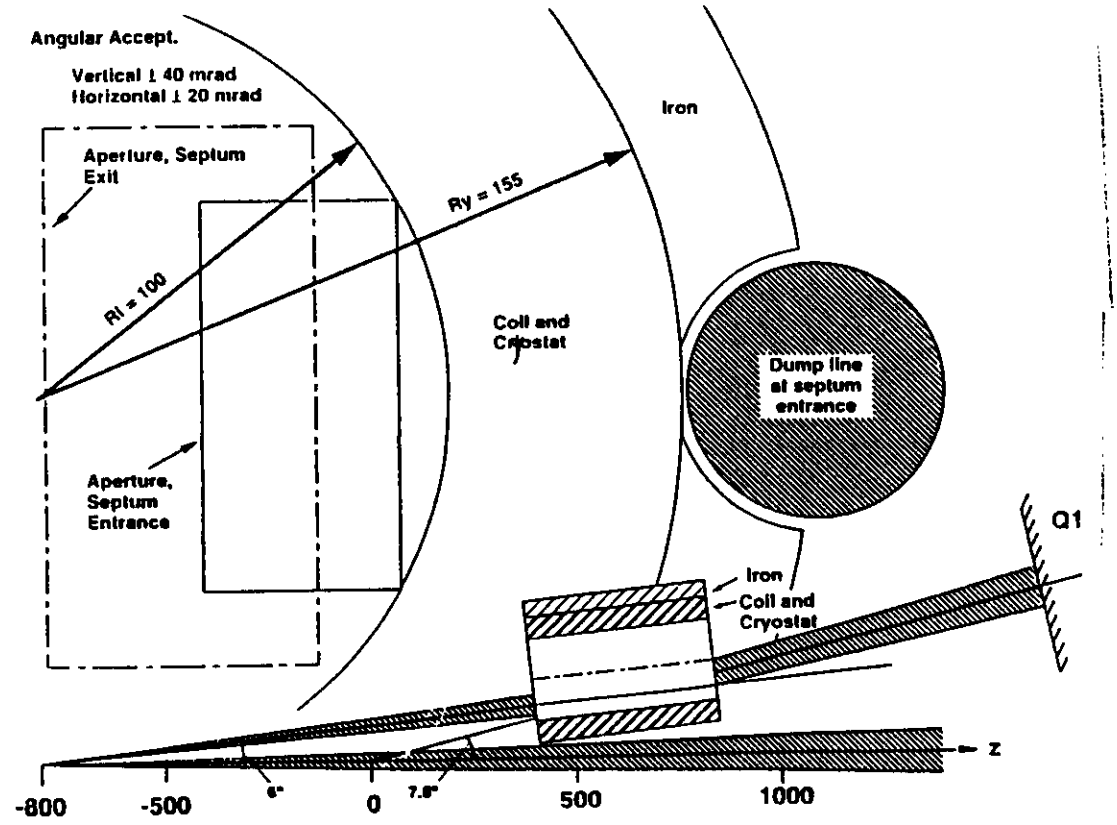

Figure 3 One superconducting Septum $\Phi = 6^\circ$, $\beta = 7.5^\circ$

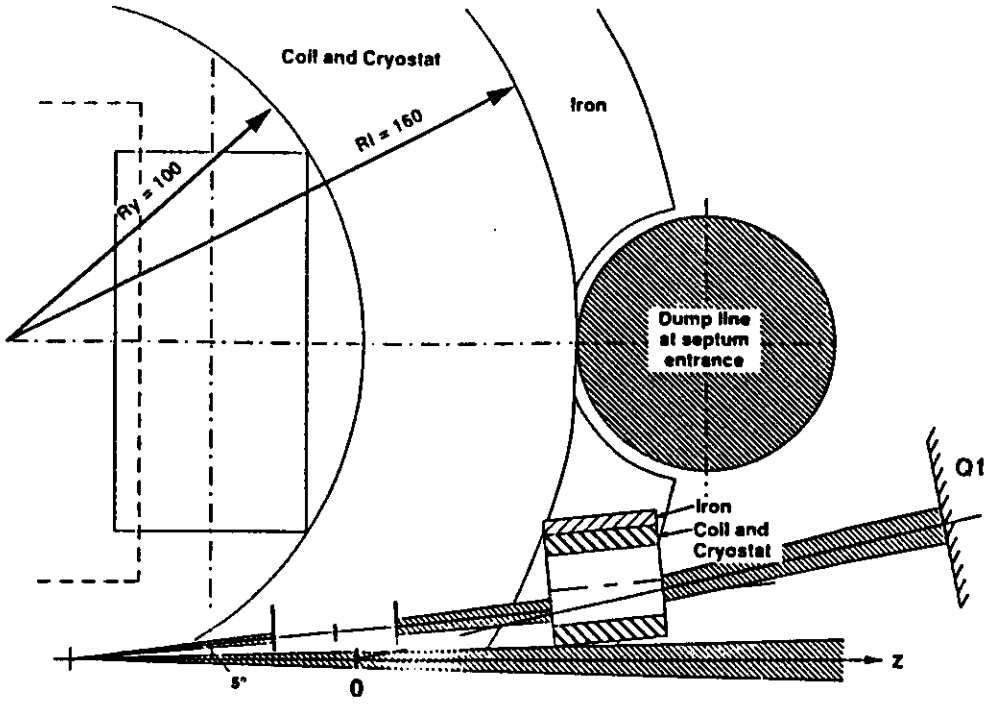

Figure 4 Room temperature Septum in front of the superconducting one

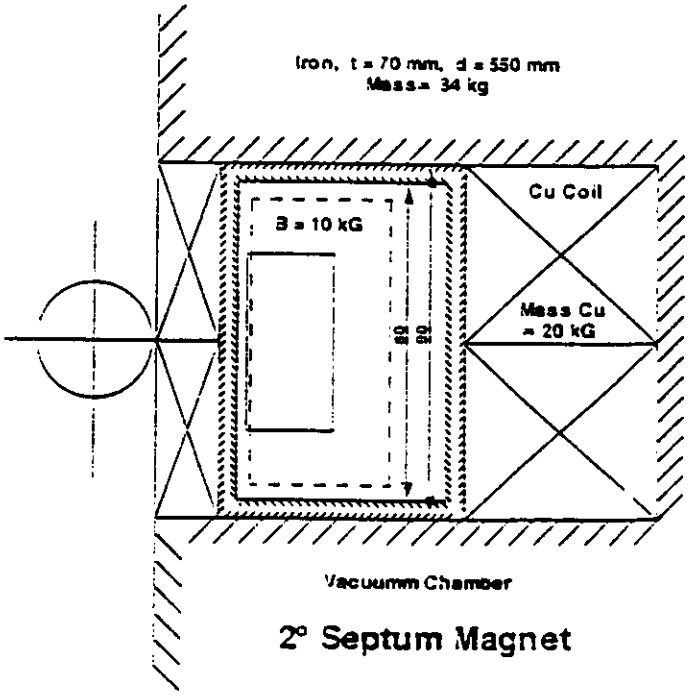

Figure 5 Second Septum Magnet $\Phi = 5^\circ$, $\beta = 7.5^\circ$

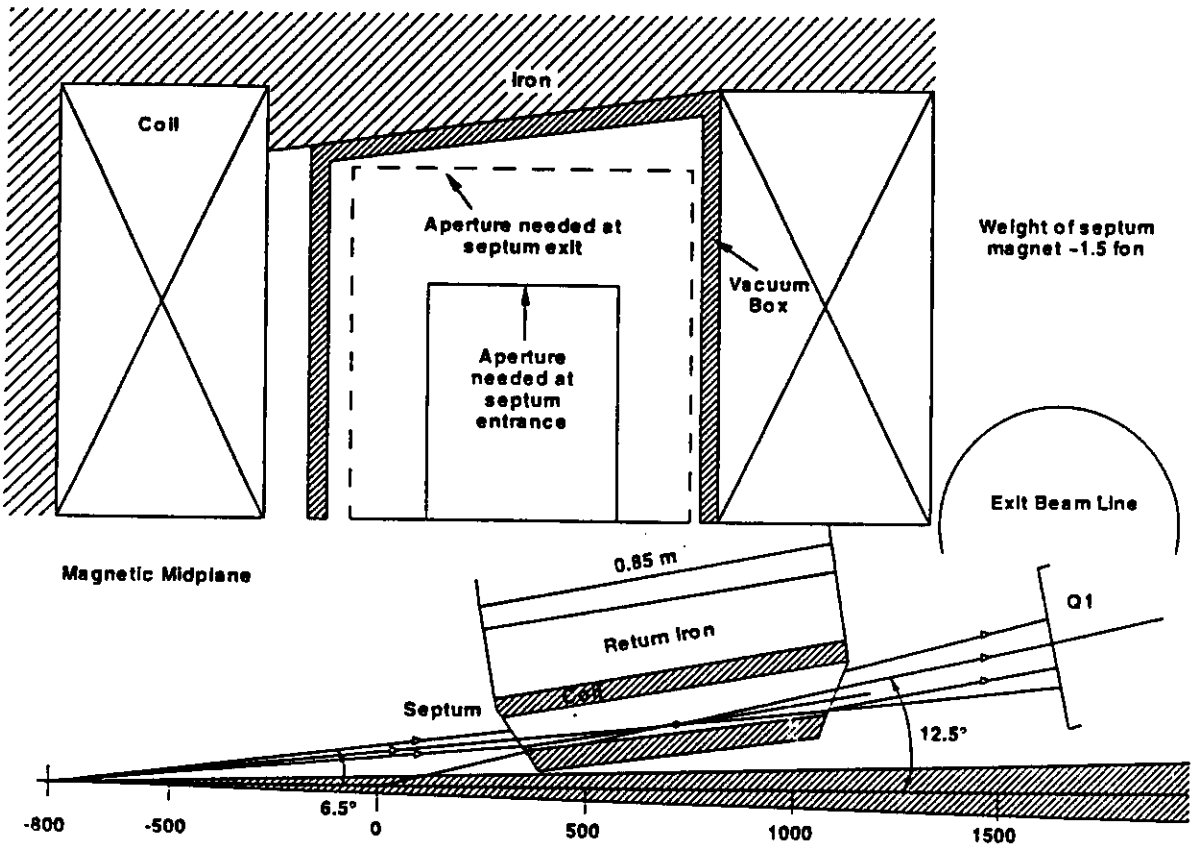

Figure 6 RoomTemperature Septum